PAPER

Check for updates

Physicochemical characterization of particulate matter in a cement production plant†

Torunn K. Ervik, [ID] [a] Stine Eriksen Hammer, [ID] *[a] Hilde Notø,[a] Dag G. Ellingsen,[a] Yngvar Thomassen,[a] Stephan Weinbruch,[ab] Nathalie Benker[b] and Balazs Berlinger [ID] ‡[a]

Employees working in cement production plants are exposed to airborne particulate matter (PM) which may lead to lung function impairments and airway symptoms. The PM consists of raw materials, clinker and additives which vary depending on cement blend. The aim of this work was to characterize the thoracic fraction of PM with regard to size, phase composition and mixing state. Both stationary and personal impactors were used to collect size-fractionated samples in a cement production plant in Norway. Stationary samples were measured with aerosol particle counters and collected with a 13-stage cascade impactor, which were stationed at three locations of the cement production plant: at the raw meal mill, clinker conveyor belt and cement mill. Sioutas cascade impactors, and thoracic and respirable dust samplers were used in parallel for personal sampling. Additionally, particles for electron microscopy were collected with the stationary cascade impactor for size-fractionated single particle characterization. Gravimetric measurements and element compositions of the samples from the stationary impactors show that the PM mass is dominated by calcium-rich particles of size >1 μm. The size distribution results of stationary and personal impactors were similar. Characterization of single particles reveals that limestone is the dominating material in the raw meal mill, whereas clinker and limestone dominate at the clinker conveyor belt and at the cement mill. The element composition of clinker PM did not change with particle size. The PM collected on impactor stages with aerodynamic diameter cut-offs below 0.56 μm was dominated by soot and volatile secondary particles at the three locations. The number of ultrafine particles of the cement related compounds was low. Air concentrations of PM in personal respirable and thoracic samples ranged from 0.14–10 mg m^{-3} to 0.37–9.5 mg m^{-3}, respectively. Considerable local variations exist, both in composition and air concentration of the PM.

Environmental significance

Cement production generates a large amount of airborne particulate matter (PM). The workers in the cement industry can be exposed at all production stages. It has previously been shown that inhalation of PM from cement production plants is linked to airway symptoms and obstructive lung changes. However, the physicochemical characteristics of PM have not yet been fully characterized in this industry. We found that the composition of the PM changes with location at a cement production plant, and that clinker and limestone particles were the main constituents of particles larger than $d_{ae} = 0.56$ μm. The number of cementitious ultrafine particles was low. The ultrafine fraction was dominated by soot and volatile secondary particles. Assessment of the variation in PM composition at cement plants is necessary to understand exposure–response association in this industry.

1. Introduction

The global cement production was estimated to be 4.1 billion tonnes in 2019 with 5.9% produced in Europe. In the year 2019,

[a]National Institute of Occupational Health, Gydas vei 8, N-0363 Oslo, Norway. E-mail: stine.hammer@stami.no

[b]Technical University of Darmstadt, Institute of Applied Geosciences, Schnittspahnstrasse 9, D-64287Darmstadt, Germany

† Electronic supplementary information (ESI) available. See https://doi.org/10.1039/d2em00139j

‡ Current address: Department of Animal Hygiene, Herd Health and Mobile Clinic, University of Veterinary Medicine, István u. 2., H-1078 Budapest, Hungary.

47 605 workers were employed in European production.[1] The main raw material for cement production is limestone, which mainly contains calcite ($CaCO_3$) and aragonite ($CaCO_3$). In addition to this calcium (Ca) source, silicon (Si), aluminium (Al) and iron (Fe) sources are necessary to obtain the right composition of the cement clinker.[2] The additional raw materials vary from *e.g.* naturally occurring clay, shale, sand and marl to industrial by-products such as slag and fly ash.[3] All raw materials are crushed, ground and milled to fine powders and mixed to form the raw meal powder. This meal is calcined in the cement kiln at a high temperature (1450 °C), which releases mainly carbon dioxide to obtain the wanted proportions of Ca, Si, Al and Fe. The product of this calcination process is named

clinker, which consists mainly of alite ($3CaO \cdot SiO_2$), belite ($2CaO \cdot SiO_2$), tricalcium aluminate ($3CaO \cdot Al_2O_3$) and calcium aluminoferrite ($Ca_2(Al, Fe)_2O_5$). Alite is the major phase, comprising on average 65% of the clinker, whereas the belite, aluminate and ferrite contents are on average 13, 11 and 8%, respectively.[4] However, these values differ based on the process and raw materials. The clinker is cooled after the cement kiln process and conveyed to the cement mill where it is mixed with a few percent gypsum ($CaSO_4 \cdot 2H_2O$) and often other additives to produce a specific cement type, and finally ground to the optimum particle size. The cumulative particle size distribution of milled clinker showed that approximately 50% of the clinker is below 15–20 μm with around 7–9% of the material smaller than 2 μm.[2]

Cement production generates large amounts of airborne particulate matter (PM) released into the workroom air. Employees in a cement production plant can be exposed to cement and/or raw material PM throughout the entire production chain, from milling of raw materials to packing of finished products. Inhalation of PM during production has been found to cause airway symptoms and obstructive lung changes.[5] Airway irritation caused by this PM has been linked to clinker mineral particles, which react with moisture to form alkaline calcium hydroxide.[6–8]

Earlier studies have observed PM geometric mean (GM) concentrations in workrooms between 0.29 and 432 mg m^{-3} for different work tasks and/or working areas' air using 'total dust' air samplers.[9–14] The "total dust" sampler has been found to sample particle sizes with a penetration curve between the thoracic and inhalable aerosol fraction.[15] Measuring the thoracic fraction is, however, more relevant for the specific respiratory effects observed in this industry.[16,17] The thoracic fraction is the mass fraction of inhaled particles that penetrate beyond the larynx with a 50% cut-off of $d_{ae} = 10$ μm, whereas the respirable fraction is the mass fraction of particles that penetrate the alveolar region of the lungs and have a 50% cut-off of $d_{ae} = 4$ μm.[18] In a large exposure assessment study including 22 cement producing plants across Europe and 6111 personal thoracic samples, the thoracic PM concentrations varied between job types from 0.20 to 1.2 mg m^{-3} (GM) with the highest air concentrations found for production, cleaning, and maintenance workers.[17]

Despite the thorough work of the previous assessments of PM workroom air concentrations during cement production, there exists little information on individual particle composition and how the elemental and phase PM compositions vary with particle size and location during production. Additional knowledge about size distribution is important since it influences both penetration and deposition in the human respiratory tract.[19] Furthermore, adverse health effects are not only associated with the mass of deposited PM, but also with its chemical and physical properties. Therefore, knowledge of physical and chemical properties of particles is fundamental to understand exposure–response associations. To the best of our knowledge, detailed characterization of the phase composition, morphology and mixing state of airborne PM generated during production has not been reported for the cement industry.

The present paper investigates the size distribution and the chemical characteristics of PM in the thoracic fraction in workroom air during cement production collected with stationary and personal sampling equipment. Personal impactors were used to compare the size distribution with that collected with the stationary impactor.

2. Materials and methods

2.1 Stationary air sampling

Stationary air sampling was performed in a cement factory in Norway during spring 2017 and fall 2018. Three different locations were investigated: raw meal mill, clinker conveyor belt and cement mill (Fig. S1, ESI†).

In spring 2017, air samples were collected with a stationary 13 stage Model 125R NanoMOUDI-II™ impactor (Microorifice Uniform Deposit Impactor; MSP corporation, TSI, Shoreview, MN, USA) on 47 mm 5 μm pore size polyvinyl chloride (PVC) filters (Merck Millipore, Burlington, MA, USA). Sampling times were 280–330 minutes, and the impactor was operated at an air flow rate of 10 L min^{-1}. The 50% cut-off sizes for particle aerodynamic diameter (d_{ae}) for each stage were 10, 5.6, 3.2, 1.8, 1.0, 0.56, 0.32, 0.18, 0.10, 0.056, 0.032, 0.018 and 0.010 μm, respectively. When referring to impactor stages in the following manuscript 50% cut-off size d_{ae} will be abbreviated to $d_{ae,50}$. Stage 1 is defined as the stage with $d_{ae,50} = 10$ μm.

The NanoMOUDI impactor was also used to collect particles for scanning electron microscopy (SEM). Copper (Cu) finder grids with holey carbon film (EMresolution, Sheffield, UK) were affixed to the surface of PVC filters and used as substrates on each impactor stage. The sampling times in this case varied between 10 and 15 minutes.

Additional measurements were performed during fall 2018 at the same positions as in the first campaign. A scanning mobility particle sizer (SMPS) instrument (model 3938, TSI Inc., Shoreview, MN, USA), equipped with an electrostatic classifier (Model 3082) with a differential mobility analyzer (Long DMA Model 3081A) and an ultrafine condensation particle counter (CPC, Model 3756), was used to count particles from 17 to 542 nm mobility diameter (d_{me}). In addition, an aerodynamic particle sizer (APS, Model 3321, TSI Inc., Shoreview, MN, USA) was operated in parallel to the SMPS in the second campaign. The APS detects particles within the size range of 0.542–19.8 μm d_{ae}. The Stokes correction in the APS software, which takes into account the particle density, was applied with a density of 2.7 g cm^{-3}[20] for the raw meal mill, whereas for the clinker conveyor belt and the cement mill, a value of 3.15 g cm^{-3} was used (density of clinker[2]). These values were based on the dominating particle types identified by SEM. After applying the Stokes correction, the size range that was measured changed to 0.542–17.15 μm. The shape-factor also influences the APS response. Since the particles are of all kinds of shapes, we have chosen to assume spherical particles and have used a shape factor of 1.0. This assumption was also used when the number distribution was converted into mass distribution.

For both the raw meal and the cement mills, the stationary NanoMOUDI impactor and the APS and SMPS aerosol particle

1244 | *Environ. Sci.: Processes Impacts*, 2022, **24**, 1243–1256

This journal is © The Royal Society of Chemistry 2022

counters were located indoor, whereas at the clinker conveyor belt the equipment was located outdoor.

2.2 Personal air sampling

Full-shift (~8 hours) personal air samples were collected in spring 2017 for 10 workers with 4-stage Sioutas cascade impactors (SKC, Eighty Four, PA, USA) with 50% particle cut-off sizes of 2.5, 1.0, 0.5 and 0.25 μm, respectively. The Sioutas impactors were loaded with 25 mm 0.5 μm pore size polytetra-fluoroethylene (PTFE) filters (Pall Corporation, Port Washington, NY, USA). Particles below the cut-off of 0.25 μm were collected on 37 mm 2.0 μm pore size PTFE after-filters (SKC, Eighty Four, PA, USA). The Sioutas impactors were operated in parallel with GK 2.69 thoracic (BGI Instruments, Waltham, MA, USA) and respirable cyclones (JS Holdings, Stevenage, UK) equipped with 37 mm 5 μm pore size PVC filters (Merck Millipore Ltd. Tullagreen, Cork, Ireland). The operators often performed their work tasks at several sections of the cement production plant. The work tasks involved cleaning with vacuum trucks, maintenance of both raw meal mill and cement mill as well as production and control related duties.

2.3 Gravimetric measurements

The PM mass was determined gravimetrically using a Sartorius Micro model MC5 balance (Sartorius AG, Göttingen, Germany) with a maximum capacity of 5.1 g and stability < 1 μg in a weighing room dedicated to low filter mass measurements (relative humidity 40 ± 2%, temperature 20 ± 1 °C). The mass detection limit, calculated as 3 times standard deviation of all field filter blanks ($n = 5$), was 0.005 mg. The PVC substrates were chosen based on their non-hygroscopicity ensuring mass stability. All filters and substrates were stored in the weighing room for at least two days, before and after exposure, for conditioning prior to weighing. All filters and substrates were discharged using a ^{210}Po source prior to weighing.

2.4 Electron microscopy

Particles collected on Cu grids using the NanoMOUDI impactor were investigated by SEM and transmission electron microscopy (TEM). A specially made TEM grid sample holder was used in SEM. Particles were imaged and their element composition

measured with a Hitachi SU6600 field emission SEM (Hitachi, Tokyo, Japan) equipped with a Bruker energy-dispersive X-ray (EDX) detector (Bruker Nano GmbH, Berlin, Germany) and a NORDIF electron backscatter diffraction (EBSD) detector (NORDIF, Trondheim, Norway). It is generally the secondary electrons that are used for imaging, while the EDX detector is used for element detection and thereby automatic analysis. Automated analysis of size, shape and elemental composition of particles was performed using the feature module of the Esprit software (Bruker nano GmbH, Berlin, Germany). In the automatic particle analysis, high contrast backscatter images were acquired from the SEM at a resolution of 1800 × 1350 pixels (pixel size = 0.03 × 0.03 μm). The whole particle was scanned during X-ray acquisition. The elemental composition (atomic%) was quantified with the Esprit software using standardless peak-to-background ZAF correction. Based on the elemental composition, shape and morphology, non-volatile particles were classified into 11 groups (Table 1). The number of particles investigated on each stage varied between 80 and 330. Soot agglomerates are not specifically mentioned in Table 1 and these fall into the C-rich particle group. However, based on the morphology, a large part of the C-rich particles are soot agglomerates, particularly for particles with $d_{ae,50} = 1$ μm (stage 5). In addition to the groups shown in Table 1, evaporating particles during electron bombardment were frequently observed. These volatile secondary particles are particles that form by condensation of gaseous precursors and their main components are sulphate, nitrate and organic carbon.[21] Such particles were excluded from further analysis, as their number abundance cannot be determined accurately. Some particles were investigated by EDX mapping analysis to identify the distribution of elements. Particles were also investigated by TEM using a Jeol 2100 F (Jeol, Tokyo, Japan) field emission gun instrument coupled with an X-Max EDX silicon drift detector (Oxford Instruments, Abingdon, UK). The microscope was operated in scanning transmission electron microscopy (STEM)[22] and TEM mode. The acceleration voltage was 200 kV leading to a point resolution of approximately 0.22 nm. Images were recorded with a charge-coupled device (CCD) camera and processed with Digital Micrograph software (Gatan Inc., Pleasanton, USA) and FIJI image processing software.[23] All Cu grids from the stationary NanoMOUDI impactor were investigated by

Table 1 Particle group classification of non-volatile particles

Particle group	Classification criteria	Additional observations
Limestone	Ca, C and O as major elements	Mg, Si, Al and Fe as minor elements
Aluminium oxide rich	Al and O as major elements	Mg, Si and F as minor elements
Silica	Si and O as major elements	
Iron-oxides	Fe and O as major elements	
Alkali sulphates	Na, K, S and O as major elements	Ca as the minor element
Clinker phases	Ca/Si, Ca/Al, and Ca/Fe ratios	
Ca sulphate	Ca, S and O as major elements	
Fly ash	Spherical morphology	Si and Al as major elements
Silicates	Si, Al, Mg, Ca, and O as major elements, non-spherical morphology	
C-rich	Dominated by C	O and S as major or minor elements
Others	Particles not assigned to the above listed groups	

This journal is © The Royal Society of Chemistry 2022

Environ. Sci.: Processes Impacts, 2022, **24**, 1243–1256 | **1245**

SEM. In addition, the Cu grids collected for $d_{ae,50} = 0.56$ μm (stage 6) were investigated by TEM.

2.5 Bulk elemental measurements

The elemental composition of PM on filters collected with the NanoMOUDI impactor was determined in solution with an Agilent 8800 inductively coupled plasma triple quadrupole mass spectrometer (ICP-MS) (Agilent Technologies, Santa Clara, CA, USA).

The filters were digested with a mixture of 65% HNO_3 (1.5 mL), 37% HCl (5 mL), 40% HF (0.6 mL) and 5 mL H_3BO_3 (puriss p.a., Sigma Aldrich-Merck, Darmstadt, Germany) in temperature-controlled vessels using a Multiwave PRO microwave oven (Anton Paar, Graz, Austria). The digests were diluted to 50 mL with 18.2 MΩ cm deionised water (Merck Millipore, Billerica, MA, USA) after adding 200 μL internal standard solution (25 mg L^{-1} Ga, Ge and In).
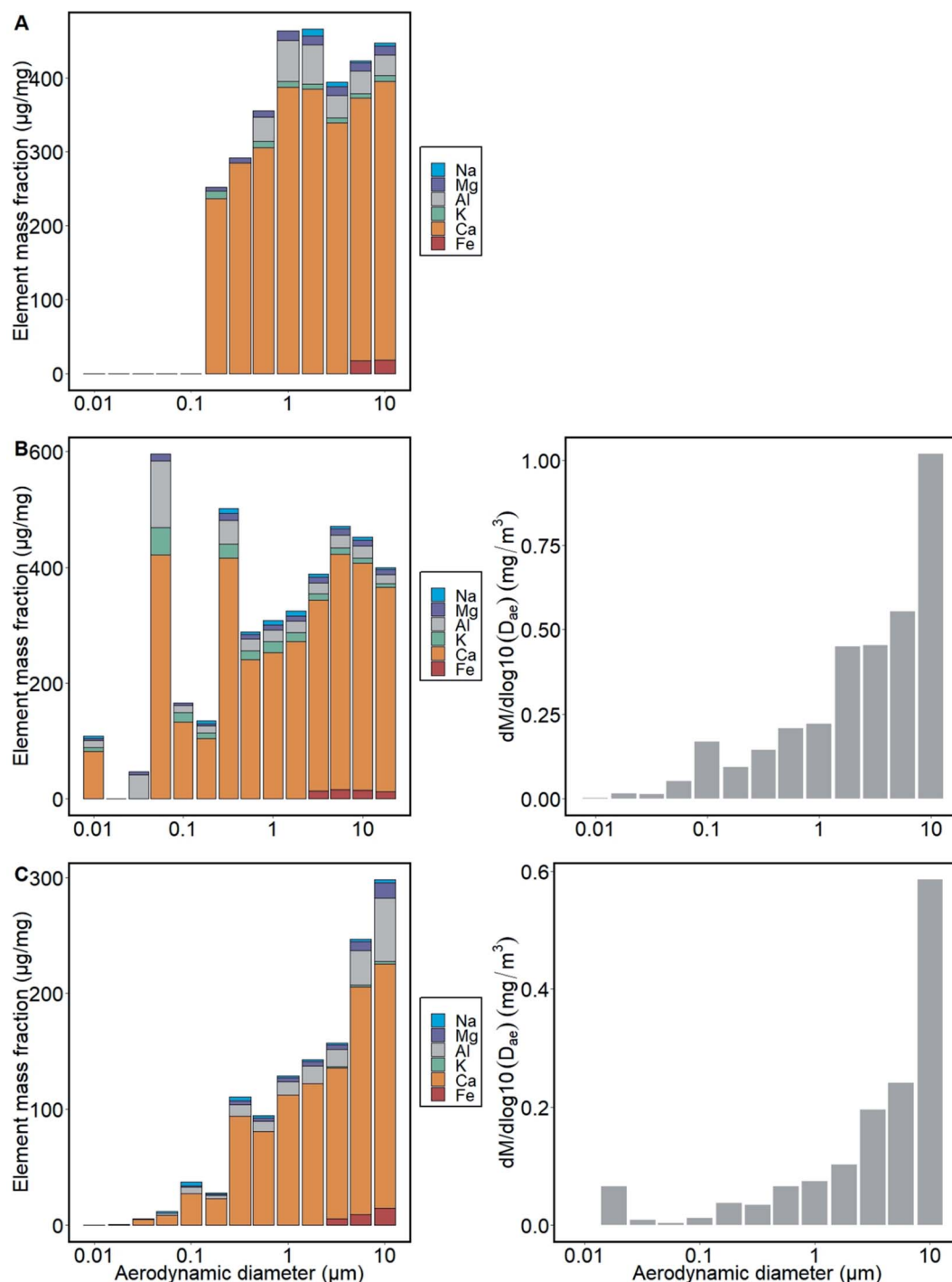

Fig. 1   Element mass (μg) relative to the PM mass on each filter stage (mg) collected close to the raw meal mill (A), clinker conveyor belt (B) and cement mill (C) with the NanoMOUDI impactor. Gravimetric mass concentrations of the respective samples are presented to the right.

1246 | *Environ. Sci.: Processes Impacts*, 2022, **24**, 1243–1256

This journal is © The Royal Society of Chemistry 2022

The ICP-MS was tuned with a matrix matched solution prior to each run, and matrix matched standards were used for calibration. Blank samples and the standard reference material Portland Cement (blended with slag and fly ash) 1881a (National Institute of Standards and Technologies, Gaithersburg, MD, USA) were prepared in the same manner as the samples. Recoveries are presented in the ESI (Table S2†).

2.6 Statistics

The relative number abundances of different particle groups are presented in Fig. 4, keeping in mind that only the ratio between two groups can be interpreted as the proportion is constrained to values between 0 and 1. The 95% confidence interval (CI) values of particle types in Table 2 were calculated in RStudio[24] using the CRAN package CoinMinD[25] using the calculation by Quesenberry and Hurst.[26] The geometric mean, minimum and maximum are shown for the PM concentration in similarly exposed groups (Table 3).

Fig. 1 was made in RStudio with the additional CRAN packages ggplot2,[27] ggpubr[28] and ggsci.[29] The rest of the figures were made using SigmaPlot (Systat Software, San Jose, CA) except for Fig. 4 which was made in Excel.

3. Results

3.1 Particle mass size distribution and size-resolved bulk elemental composition of stationary samples

The PM and elemental mass distributions of NanoMOUDI samples collected at the clinker conveyor belt and at the cement mill are displayed in Fig. 1. Elemental mass distribution is related to the total mass measured on each filter stage in NanoMOUDI. Concentrations below the limit of detection (LOD) are not included in the figure. Gravimetric results from the raw meal mill are not shown because these samples were most probably contaminated by lubricant oil from the seal rings. A high amount of PM, >40% in the cement mill and 30% at the clinker conveyor belt, is found with $d_{ae,50} = 10$ μm (stage 1). The elemental mass distribution illustrates that most of the PM is Ca-rich with minor amounts of Na, Mg, Al and Fe. The smallest size bins contain particles of other origin, as these do not include the major and minor elements related to cement particles.

Number concentrations measured with SMPS and APS, averaged over the measurement period, for the three sampling locations are displayed in Fig. 2A and B, respectively. Calculated mass concentrations from APS number concentrations are shown in Fig. 2C. With the parameters applied in this study, the d_{me} of particles counted with SMPS ranged from 17 to 542 nm. The highest particle number concentrations were found in the raw meal mill with 2×10^4 cm^{-3} for particles of 60 nm size. The shape of the distribution curve from the cement mill shows a bimodal distribution with peaks at 50 nm and 300 nm. A bimodal distribution is also observed for the clinker conveyor belt, with peaks at 25 nm and 400 nm.

Values up to 1300 cm^{-3} and 500 cm^{-3} averaged over the measurement period were measured for the cement mill and the raw meal mill for larger particles (0.5–20 μm). The size distribution is shifted towards $d_{ae} = 1$ μm for the cement mill
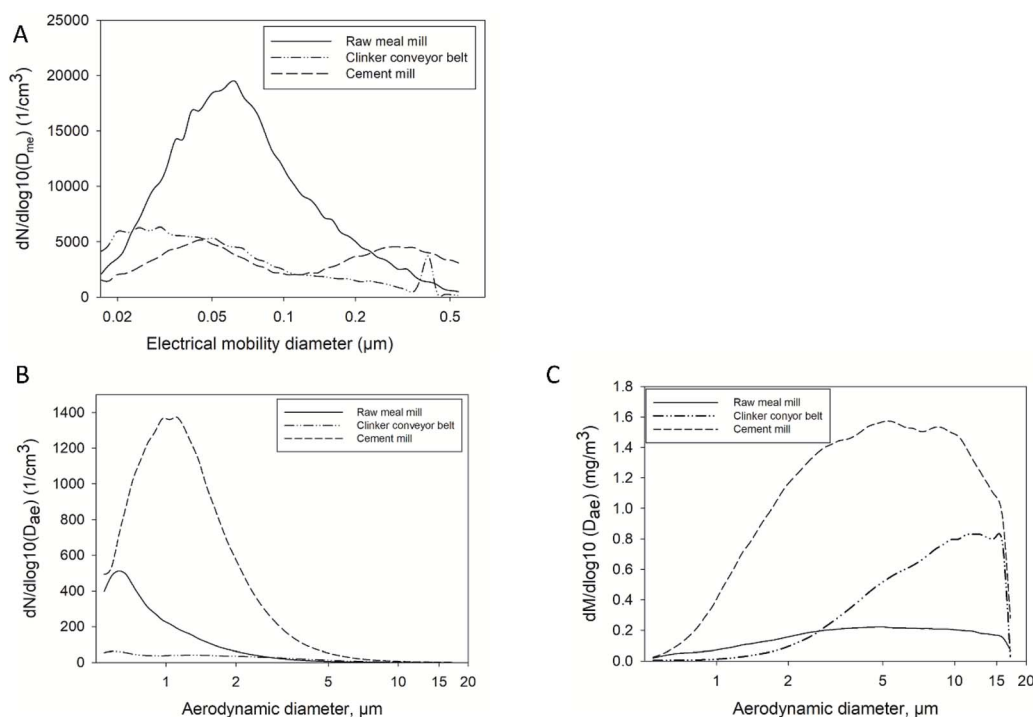

Fig. 2 SMPS average number concentrations for the raw meal mill, clinker conveyor belt, and cement mill (A), APS average number concentrations for the raw meal mill, clinker conveyor belt, and cement mill (B) and calculated average mass concentrations from APS data for the raw meal mill, clinker conveyor belt, and cement mill (C).
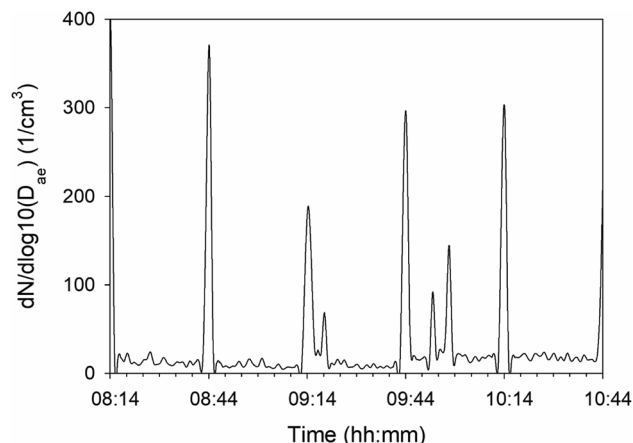
This journal is © The Royal Society of Chemistry 2022

Environ. Sci.: Processes Impacts, 2022, **24**, 1243–1256 | **1247**

Fig. 3 APS number concentration for $d_{ae} = 2.46$ μm as a function of time measured at the clinker conveyor belt.

compared to that of the raw meal mill and conveyor belt where most particles are close to $d_{ae} = 0.6$ μm. The number concentrations in the cement mill led to average mass concentrations close to 1.6 mg m^{-3} for particles in the size range d_{ae} 5–10 μm. Compared to the indoor locations, raw meal mill and cement mill, the number concentration values measured at the clinker conveyor belt were lower with the highest mean value measured to be 60 cm^{-3}. Nevertheless, the variability measured with APS

at the clinker conveyor belt showed a distinct pattern with peak events every 30 min with values up to 350 cm^{-3} (Fig. 3).

3.2 Single particle characterization by electron microscopy

In the following, the main particle groups observed in the three investigated sections are described in detail. The relative number abundances of non-volatile particle groups encountered on the first seven stages ($d_{ae,50} = 10$–0.32) in the Nano-MOUDI impactor are shown in Fig. 4. Stages 8–13 ($d_{ae,50} = 0.18$–0.010 μm) are not included in the figure because these stages were dominated by soot agglomerates and volatile secondary particles, and the latter ones evaporated under electron bombardment. The EDX spectra for volatile secondary particles included C from the substrate and a small S peak, which disappeared with time.

3.2.1 Raw meal mill. Up to 80% of non-volatile particles found in the size range $d_{ae,50} = 10$ μm–0.56 μm was limestone (Fig. 4). The limestone particles often contained inclusions of various other phases as can be seen in the element distribution images (Fig. 5). In addition to limestone particles, ~30% of Al–O-rich particles (Fig. 6A) were found (~30%), particularly in the sizes $d_{ae,50} = 10$ μm and 5.6 μm (stages 1 and 2). These particles often contained Mg, Si and F as minor elements. Some Si–O rich, presumably quartz particles (3–8%) were identified. Approximately 4% of the particles analyzed on the seven stages were Si–O rich. Fe–O rich particles were rare (≤2%).
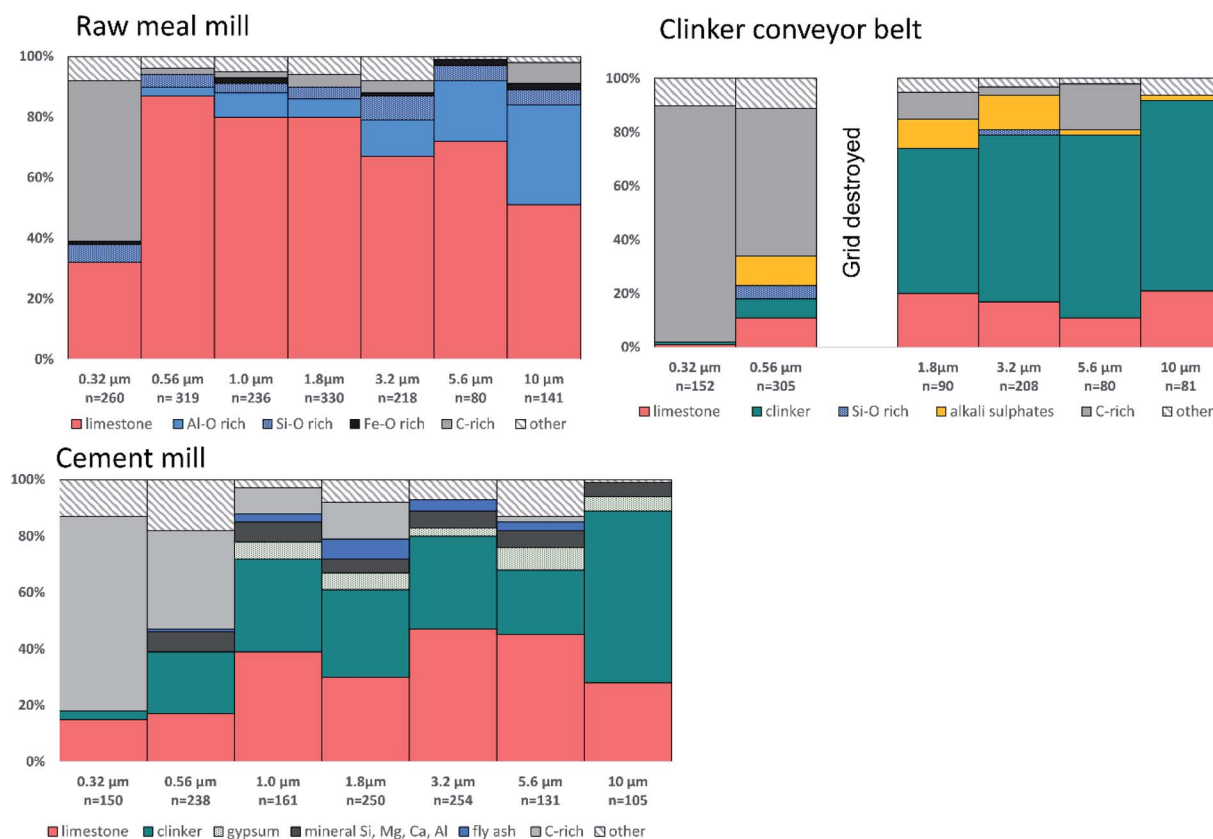

Fig. 4 Relative number abundances of particle groups in the size range $d_{ae,50} = 0.32$–10 μm (stages 7–1) collected using the NanoMOUDI impactor from the raw meal mill, clinker conveyor belt, and cement mill. Volatile particles are not included.
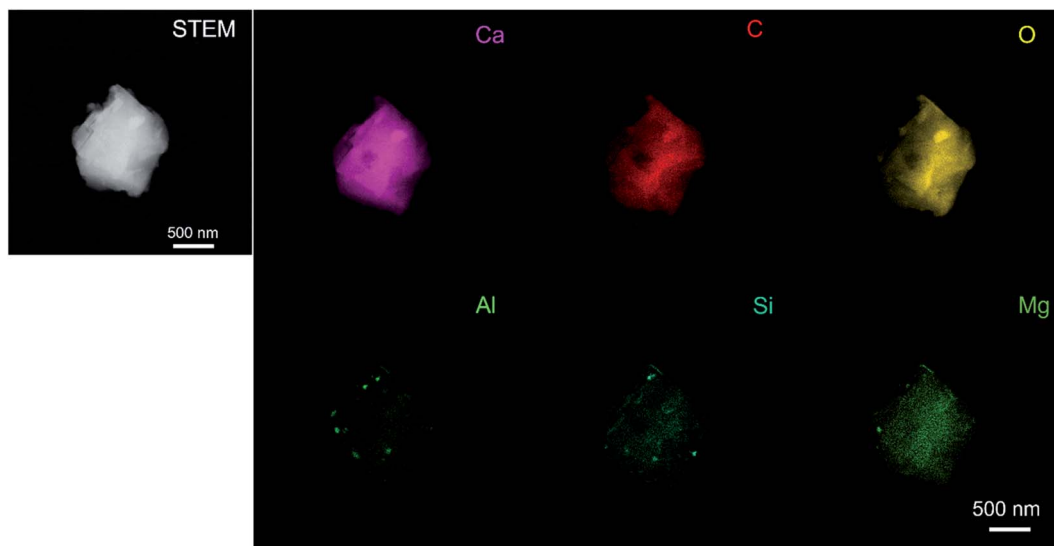
1248 | Environ. Sci.: Processes Impacts, 2022, 24, 1243–1256

This journal is © The Royal Society of Chemistry 2022

Fig. 5 STEM image and element distribution images for Ca, C, O, Al, Si and Mg of a limestone particle collected at stage 6 with 50% cut-off $d_{ae,50}$ = 0.56 μm in the stationary NanoMOUDI impactor.

In the size range $d_{ae,50}$ = 0.32–0.18 μm (stages 7 and 8) carbonaceous particles such as soot agglomerates dominated (Fig. 6B). Limestone particles still frequently occurred for $d_{ae,50}$ = 0.32 μm (32%). In the stage below $d_{ae,50}$ = 0.18 μm, however, only some limestone particles were found. Traces of volatile secondary particles were observed which probably originated from combustion sources.[30]

The dominating particle groups below $d_{ae,50}$ = 0.18 μm (stage 8) were C-rich such as soot agglomerates and volatile secondary particles. Sodium chloride (NaCl) and potassium chloride (KCl) particles were also observed. The NaCl particles, 30–100 nm in geometric diameter, were observed in a halo around some of the limestone particles (Fig. 6C). They were most likely formed by evaporation of sea water droplets[31] since the cement factory is located by the sea. Spherical particles of Fe oxide, identified to contain magnetite by SEM-EBSD, occurred for $d_{ae,50}$ = 0.18 μm (stage 8), but these were rare.

3.2.2 Clinker conveyor belt. The dominating group of non-volatile particles in the size range $d_{ae,50}$ = 10–1.8 μm (stage 1–4) was classified as clinker. Particles consisting solely of alkali sulphates were also present (Fig. 6D). Some clinker particles are covered by KCl particles (Fig. 7). Particles containing traces as well as higher amounts of both lead (Pb) and zinc (Zn) were also observed and occurred more often in the size ranges below $d_{ae,50}$ = 1 μm (stage 5). Below this stage, a high fraction of the particles observed were C-rich, mainly as soot agglomerates. In addition, clinker, limestone and alkali sulphates were often observed for $d_{ae,50}$ = 0.56 μm (stage 6). In the soot agglomerates investigated by TEM no metal inclusions were found. For $d_{ae,50}$ = 0.32 μm and 0.18 μm (stages 7 and 8), only some clinker and limestone particles were found. Below $d_{ae,50}$ = 0.18 μm (stage 8) clinker was rare. Some volatile secondary particles were observed on these stages.

3.2.3 Cement mill. Clinker (>50%) and limestone (∼30%) were the dominating particle groups observed for $d_{ae,50}$ = 10 μm

(stage 1) at the cement mill. The abundance of limestone particles relative to clinker particles increased for $d_{ae,50}$ = 5.6 (stage 2) and 3.2 μm (stage 3). Fly ash particles (Fig. 6E) were only observed at the cement mill and are identified based on their aspect ratio.[32]

In addition to fly ash, irregular non-spherical particles with similar element composition were observed which might be bottom ash particles or other mineral particles. These are classified as silicates. Some Ca sulphate particles (gypsum) were identified (Fig. 6F).

For $d_{ae,50}$ = 0.56–0.32 μm (stages 6 and 7), a higher fraction of C-rich particles (mostly soot) was observed. Volatile secondary particles were also frequently encountered in this size range. Their abundance is possibly underestimated in the automatic analysis because of low contrast. These volatile secondary particles observed at the cement mill were slightly larger than those found around the clinker conveyor belt and in the raw meal mill.

Carbonaceous particles such as soot and volatile secondary particles dominated at sizes below 50% cut-off $d_{ae,50}$ = 0.18 μm (stage 8). A few spherical amorphous Si–O rich particles were also observed below this stage.

The number abundance of the various clinker phases was assessed by scanning the entire clinker particles with EDX. Based on the Ca/Si, Ca/Al and Ca/Fe ratios, the particles were classified as alite, belite or tricalcium aluminate and calcium aluminoferrite. As many of the larger particles were polyphased, the analysis will only give an indication of the dominating phase. The relative number abundances of the four major clinker phases collected on the stages with 50% cut-off $d_{ae,50}$ = 10 μm, 1.8 μm and 0.56 μm at the cement mill are given in Table 2.

3.3 Particle mass concentrations of personal samples

Air concentrations of PM in samples collected with personal thoracic, respirable cyclones and Sioutas impactors are shown
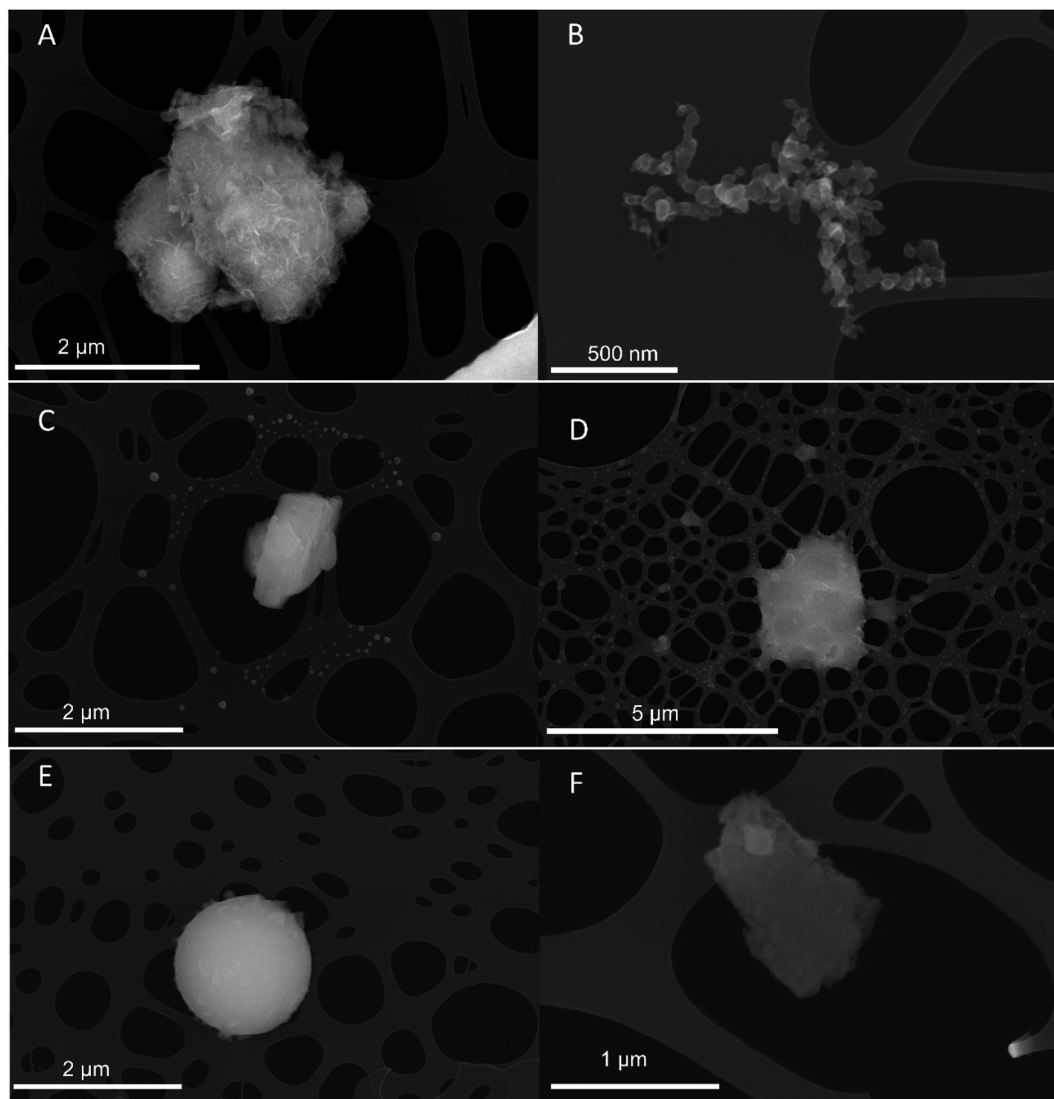
Fig. 6 Typical secondary electron images of (A) Al−O-rich particles, (B) soot agglomerates, (C) limestone, (D) alkali sulphates, (E) fly ash, and (F) Ca sulphate.

in Table 3. Similar exposed working groups (SEG) are defined based on the work task, which may be performed in different areas of the cement plant. The PM air concentrations varied strongly within each SEG, with the highest variation found among the maintenance workers. Production workers had the highest geometric mean in the PM size fractions below 0.5 μm. The calculated thoracic and respirable fractions from the Sioutas impactor are found in Table S3 in the ESI.†

4. Discussion

4.1 Size distribution of PM

4.1.1 SMPS and APS number concentrations. Number concentrations measured with SMPS in the size range 17–542 nm are relatively low compared to those of measurements performed in other industrial environments such as Mn alloy and SiC smelter halls.[33,34] This is probably the case because most PM were generated by mechanical crushing and grinding processes in the cement plant, whereas in the referred studies measurements were performed close to the furnaces and the thermal processes. The ultrafine particles observed in the cement plant were predominantly soot and volatile secondary particles, which most likely originated from the use of fuel and waste as energy sources for heating the cement kiln. The shapes of the SMPS size distribution curves at the clinker conveyor belt and the cement mill show a bimodal distribution which may indicate that the PM stemmed from multiple sources or that there is a nucleation–accumulation mode typically found in combustion processes.[35]

The number concentrations of particles in the size range 0.542–17.15 μm measured with the APS at the cement mill and raw meal mill are plausible since crushing and grinding processes take place in the two mills. There is a relatively large discrepancy between the calculated PM air concentrations from APS data with the amounts collected with NanoMOUDI at the cement mill. As the measurements took place during two
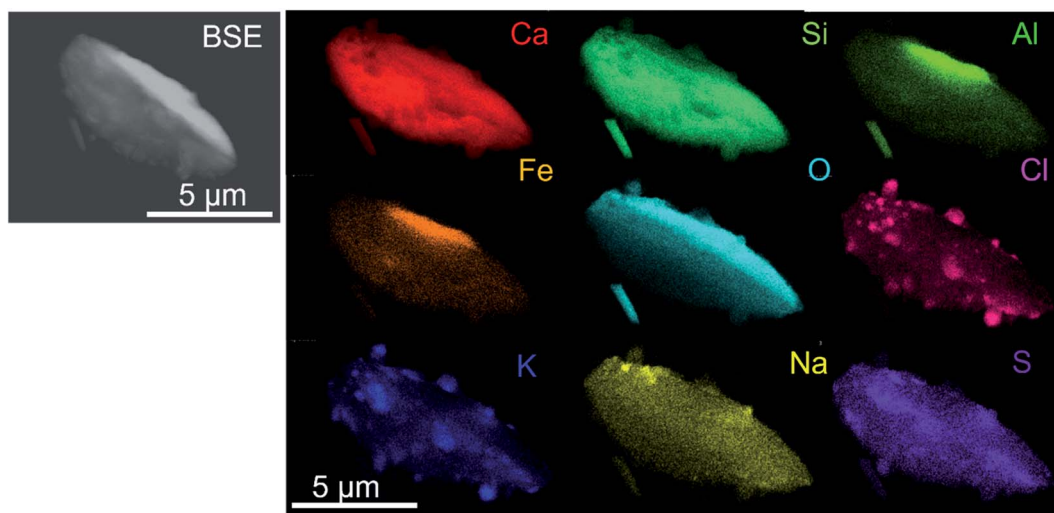
1250 | *Environ. Sci.: Processes Impacts*, 2022, **24**, 1243–1256

This journal is © The Royal Society of Chemistry 2022

Fig. 7 Backscatter electron (BSE) image and element distribution images for Ca, Si, Al, Fe, O, Cl, K, Na and S of a polymineralic clinker particle collected for $d_{ae,50} = 1.0$ μm in the stationary NanoMOUDI impactor.

Table 2 Relative number abundances of clinker minerals observed on stages 1, 4 and 6 of the stationary NanoMOUDI impactor at the cement mill

50% cut-off $d_{ae,50}$ and stage	N^a	Alite (%)	Belite (%)	Calcium aluminoferrite (%)	Tricalcium aluminate (%)
10 μm (stage 1)	59	70 [51–83]	10 [3–26]	15 [6–32]	5 [1–20]
1.8 μm (stage 4)	88	66 [51–78]	22 [13–37]	6 [2–17]	6 [2–17]
0.56 μm (stage 6)	49	72 [51–85]	12 [4–30]	10 [3–28]	6 [1–23]

^{a} N = number of particles investigated. The 95% confidence interval values are shown in brackets.

sampling campaigns, it may be suspected that the PM mass concentrations at the cement mill show a large variation with time. In contrast, the calculated PM mass concentrations from APS data at the clinker conveyor correspond well to the measured PM values from NanoMOUDI. It can also be seen that the calculated mass concentrations reach higher values for the clinker conveyor belt than for the raw meal mill due to a higher

number of larger particles ($d_{ae} > 2.9$ μm). The APS time series for the clinker conveyor belt showed concentration peaks every 30 min (Fig. 3). These concentration episodes were also observed for the SMPS time series, however, not as clear as for the APS. This can be related to the cleaning cycles of the electrostatic precipitators, which are associated with high amounts of PM emitted during cleaning[36] and may explain why the mass

Table 3 Mass concentrations (mg m^{-3}) of personal samples collected in the cement production plant

Similar exposed groups		Thoracic	Respirable	Sioutas impactor [50% cut-off d_{ae} μm]				
				2.5	1.0	0.5	0.25	<0.25
Production $n = 3$	Geometric mean	1.4	0.48	1.5	0.69	0.14	0.11	0.44
	Min	0.53	0.23	0.088	0.074	0.025	0.034	0.14
	Max	3.3	1.0	10	3.4	0.45	0.31	2.0
Maintenance $n = 4^a$	Geometric mean	1.9	0.9	1.5	0.51	0.12	0.057	0.20
	Min	0.89	0.28	0.34	0.084	0.021	0.017	0.075
	Max	9.5	10	17	7.9	2.9	0.059	1.4
Cleaning $n = 5^b$	Geometric mean	2.0	0.70	1.6	0.46	0.16	0.093	0.52
	Min	0.37	0.14	0.20	0.058	0.019	0.012	0.12
	Max	4.5	1.8	4.9	1.2	0.41	0.81	3.4

^{a} $n = 3$ Sioutas impactor samples. ^{b} $n = 4$ impactor samples.

This journal is © The Royal Society of Chemistry 2022

Environ. Sci.: Processes Impacts, 2022, **24**, 1243–1256 | **1251**

concentrations of PM at the outdoor clinker conveyor belt were relatively high. In addition, trucks and cars were passing not far from the conveyor belt and resuspension of settled dust may have contributed significantly to the outdoor concentrations.

4.1.2 NanoMOUDI mass distribution and element composition. Mass distributions often show a log normal distribution. This is not the case for the mass distributions shown in Fig. 1. The NanoMOUDI impactor used in this study has an inlet which is reported to have a nominal cut-off size of 10 μm. Airborne particles at the cement plant may be larger than this, as seen in Fig. 2 B and C, and Fig. 1 therefore shows the tail of the mass size distribution. Nevertheless, the focus of our study was on the thoracic aerosol fraction. Sampling artefacts, such as fine particle loss and bouncing, may occur when using cascade impactors. Bouncing effects are especially a concern for the stages with small cut-off sizes because of high impaction velocity.[37–39] Sampling artefacts will depend on the aerosol, the type of filter used, sampling conditions and on whether grease is used or not. Investigations by Cena *et al.*[40] on the collection of welding fume samples indicated that PVC filters without grease presented minimal particle bouncing on the NanoMOUDI stages. A limitation of our study is that PM was only collected for one day at each location. The PM concentrations at the plant will vary and depend on factors such as weather and season. The PM collected at the outdoor clinker conveyor belt location will probably be affected the most by these factors. Nevertheless, the focus of this study was to investigate the PM size distribution, which may be more constant than the actual PM concentrations.

The concentrations of the main elements Al, Ca, potassium (K), Fe, Mg and Na decrease with particle size down to $d_{ae,50} = 0.32$ μm. This is consistent with what was detected in SEM, where instead C-rich particles dominate the lowest size bin (Fig. 4). The two mills (raw meal mill and cement mill) show a similar trend, that is, decreasing amount of Ca-rich particles with decreasing $d_{ae,50}$ size. However, samples collected close to the clinker conveyor belt include higher amounts of Ca, Al, K and Mg in size bins down to $d_{ae,50}$ of 0.032 μm. The higher amounts of these elements detected in the lower size bins may also originate from the cleaning cycles at the clinker conveyor belt resulting in a higher particle number concentration every 30 minutes at this site (Fig. 3).

4.1.3 Size fractionated particle groups obtained with NanoMOUDI. In general, the abundance of the different particle groups reflects the production processes in cement plants. The dominating particle groups were limestone and corrective materials such as Al–O rich and Fe–O rich particles in the raw meal mill, clinker particles around the clinker conveyor belt, as well as clinker particles and other additives (*e.g.* limestone, gypsum and fly ash) at the cement mill. Below $d_{ae,50} = 0.56$ μm (stage 6), carbonaceous and secondary volatile particles dominated and the abundance of particles from the raw material and clinker was lower.

4.1.3.1 Raw meal mill. Cement producers seek to use alternative raw materials such as industrial waste-products to meet the desired chemical composition, both to reduce costs and as a way of more environmentally friendly production. For example, recovered alumina from aluminium slags is often used instead of bauxite in clinker production.[41] The main mineralogical components of high-alumina secondary raw materials are corundum (Al_2O_3) and spinel ($MgAl_2O_4$);[42] the latter may explain the relatively high Mg content found in these particles. Furthermore, pyrite cinder (FeS_2), the remaining slag after burning pyrite, consists mainly of the oxides hematite (Fe_2O_3) and magnetite (Fe_3O_4) and is used as an alternative source of iron oxide.[43] The occurrence of ultrafine spherical particles of magnetite may thus be related to the use of pyrite cinder.

4.1.3.2 Clinker conveyor belt. Volatile K, Na, Cl and S compounds can circulate in the kiln system originating from *e.g.* the raw meal or fuel in the hotter parts of the kiln.[44] Sulphur dioxide (SO_2) can react with Na, K and Ca to form the sulphates Na_2SO_4, K_2SO_4, $CaSO_4$, $3K_2SO_4 \cdot Na_2SO_4$, and $K_2SO_4 \cdot 2CaSO_4$, which may get incorporated in the clinker.[45] These compounds can also leave the cement kiln as fine PM or form coatings on kiln surfaces. A bypass is often installed for reducing the intensity of the chloride cycle with the aim of avoiding kiln deposits. In that case, hot gas is withdrawn from the kiln and quenched with subsequent condensation of KCl vapour to solid KCl on the surface of larger PM that are further collected with filters.[46] The presence of such particles on the surface of the clinker PM in addition to the observation of limestone and alkali particles might suggest that part of the collected particles at this location was cement kiln dust (CKD),[47] which consists of fine particles from the cement kiln collected in a bag house or electrostatic precipitators. The PM peak episodes observed in the APS also indicate that CKD is a major contributor of PM around the clinker conveyor belt (Fig. 3). The main components of CKD are reported to be partially calcined raw material, clinker and alkali compounds.[48] Alternative fuels and raw materials may introduce traces of Pb and other metals into the clinker. Particularly secondary raw materials, such as dusts from steel work, have been found to be relevant for the input of Pb and Zn.[22]

4.1.3.3 Cement mill. Upon entering the cement mill, gypsum ($CaSO_4$), limestone, Fe sulfate and fly ash can be added to the clinker for the production of different cement blends. The measured fractions of gypsum, fly ash and other particle groups were low (<10%) compared to the amount of limestone and clinker. The high percentage of limestone present at the cement mill is unexpected. Portland cement, which is the most used cement, is reported to contain more than 90% clinker (5% gypsum and only 5% other ingredients). Limestone could be used as an additive in larger amounts (5–15%) in other types of cement.[49] This may be a reason for the relatively high limestone content found at the cement mill and may have been affected by the type of cement blended during the day of measurements.

Alite is more brittle than the other three clinker phases. Fracture occurs mainly through alite grains and not through phase boundaries resulting in polyphase particles after grinding[50] and the relative amount of the different phases might therefore vary with particle size. Alite reacts much more quickly with water than belite[2] and a size variation may therefore be important for the behavior in the respiratory system. However,

1252 | *Environ. Sci.: Processes Impacts*, 2022, **24**, 1243–1256

This journal is © The Royal Society of Chemistry 2022

our results (Table 2) indicate that there is no clear tendency in the relative amounts between alite and belite between stages 1–6. The relative number abundances of the different clinker minerals shown in Table 2 are based on a limited number of particles, and can, thus, only be regarded as an order of magnitude estimate. X-ray diffraction analysis of bulk samples should be used for a more thorough assessment of the relative amount of clinker phases.[51] Compared to clinker, limestone is easier to grind and tends to be ground to smaller particles.[52] Limestone particles were found in relatively high amounts (>15%) below $d_{ae,50} = 0.5$ μm.

4.2 Personal measurements using Sioutas impactor, respirable and thoracic aerosol samplers

The number of personal air samples collected was small. Thus, our results are regarded as a preliminary estimate of the mass size distribution of personal air samples. Nevertheless, to the best of our knowledge, personal impactors have not been previously used to collect PM in the cement industry. PM mass concentrations collected using personal respirable and thoracic cyclones were in the same range as reported in earlier studies[16] which shows that the Sioutas measurements are representative for the typical exposure. The GM values presented in Table 3 show that most of the PM are collected on the first and second stage in the Sioutas impactor. Compared to the stationary NanoMODUI impactor, the size distributions of the Sioutas impactors show a similar trend, with most of the PM collected in the size range $d_{ae} = 1$ μm and above. The first stage with a 50% cut-off at $d_{ae,50} = 2.5$ μm is reported to collect particles in the size range 2.5 μm–10 μm.[53] However, in laboratory tests the impactor was only tested with particles up to 10 μm and the impactor probably collects larger particles as well. The impactor is of limited use for measuring the mass size distribution of PM in the extrathoracic aerosol fraction since the aspiration efficiency of the sampler is unknown. Bau and Witschger[54] have estimated the aspiration probability of the Sioutas impactor to be as high as about 90% for $d_{ae} = 40$ μm with decreasing probabilities to about 10% for d_{ae} 80 μm. Thus, the mass collected at stage 1 is highly dependent on the presence of coarse PM. Berlinger et al.[33] found a relatively good correlation between the calculated respirable mass from Sioutas and that measured with respirable cyclones in a manganese smelter. The calculation of the respirable mass from Sioutas assumes an upper size limit of $d_{ae,50} = 10$ μm for the first stage. This assumption may be acceptable in environments where the PM mainly consists of particles with $d_{ae,50} < 10$ μm. However, collected particles with sizes larger than $d_{ae,50} = 10$ μm will shift the calculated respirable mass to higher levels. In conclusion, the Sioutas impactor can be used in the cement industry to estimate the size distribution curve of PM for particles below 2.5 μm (stage 2). Since the aspiration efficiency of the inlet is unknown, the Sioutas impactor cannot be used to estimate respirable and thoracic fractions in this industry. Personal samples collected using conventional samplers in this study show large variations in personal exposure ranging from 0.14–10 mg m^{-3} for respirable samples to 0.37–9.5 mg m^{-3} for

thoracic samples. This is comparable to the findings of Notø et al.[55] In their study, production, cleaners, and maintenance workers were the highest exposed groups. In addition, 5 out of 12 of the thoracic samples, normalized to 8 hours, are above the limit value for lung function decline of 1.56 mg m^{-3} estimated by Nordby et al.[56]

4.3 Implications of results

Lung penetration and deposition strongly depend on particle size. Samples from Sioutas, NanoMOUDI and calculated data from APS demonstrate that the PM mass is dominated by particles with d_{ae} larger than 1 μm. Cement clinker is hygroscopic and will absorb water when exposed to the high relative humidity of the respiratory tract resulting in some particle growth, which will affect both the penetration and deposition behavior in the respiratory tract. Considering salt particles, it has been found that growth takes place in about 10^{-2} s with temperatures and relative humidity of 37 °C and 99.5%, respectively.[57] Particles with a size around $d_{ae} = 1$ μm have a low deposition efficiency in the respiratory tract.[19] If these particles are hygroscopic they may grow, upon inhalation, into a size with a larger deposition efficiency.

Single particle characterization by electron microscopy showed that clinker and limestone dominate the composition of the PM at the cement mill and at the clinker conveyor belt. In the raw meal mill, limestone dominated, and the number of clinker particles was low, as expected. Employees often work in different areas of the cement production plant during a shift. Thus, our results only yield an approximate estimate of the share of different particles which workers are exposed to. Depending on work task and location, the composition of the PM will comprise a mixture of the particles shown in Fig. 4. Exposure to limestone has been found to cause respiratory symptoms such as cough during day and night.[58] Compared to clinker, however, limestone has a low aqueous alkalinity (pH 8–9).[59] Thus, the higher alkalinity of clinker particles may be more important for the lung function decline observed in this industry.[60] The amount of the various clinker phases did not change with particle size indicating that clinker particles depositing in the different regions of the lung have the same chemical and phase composition. The relatively high fraction of limestone found, not only in the raw meal mill, reveals that the total Ca content cannot be chosen as a marker for the clinker content in the PM. Another known health hazard in cement production is crystalline silica (quartz). At the raw meal mill, a total fraction of 4.2% Si–O rich particles (presumably quartz) were identified. Still, the mass concentration is unknown and should be assessed by X-ray diffraction of PM collected in the breathing zone of the workers to evaluate the exposure to respirable quartz.

In conclusion, the composition of the PM varies with location in a cement production plant with clinker and limestone particles being main constituents of particles with $d_{ae,50}$ larger than 0.56 μm. The number of ultrafine cement related particles was low, and this fraction was dominated by soot and volatile secondary particles. The amount of PM in air also varies over the

This journal is © The Royal Society of Chemistry 2022

Environ. Sci.: Processes Impacts, 2022, **24**, 1243–1256 | **1253**

day, and certain work operations at the plant may result in high air concentrations.

Author's contribution

TE performed sampling and SEM analysis and wrote the manuscript, SEH analysed the samples by ICP-MS, performed data analysis and participated in discussion of the results and manuscript writing. HN participated in sampling and discussion of the results and manuscript writing. DGE and YT took part in the study initiation, participated in discussion of results as well as preparation and review of the manuscript. SW helped with statistical analysis, participated in discussion of the results and manuscript writing. NB carried out the TEM analyses. BBE performed sampling and was engaged in the study design, discussion of the results as well as manuscript preparation and review.

Funding

Conflicts of interest

There are no conflicts of interest to declare.

References

1 CEMBUREAU, *Activity Report*, The European Cement Association, Brussels, Belgium, 2020.

2 H. F. W. Taylor., *Cement Chemistry*, UK Thomas Telford Publishing, London, 1997.

3 J. J. Thomas and H. M. Jennings. *The Science of Concrete*, Northwestern University, Evanston, IL, USA, 2009.

4 H. Justnes and C. J. Engelsen, *Environmentally Sound Management of Hazardous and Industrial Wastes in Cement Kilns - Waste as Alternative Raw Materials*, SINTEF report, Trondheim, Norway, 2007.

5 HSE, *EH75/7 - Portland Cement Dust: Hazard Assessment Document*, 2006.

6 H. Ahmadi, C. Durrant, K. Sarraf and M. Jawad, Chemical burns: A review, *Current Anaesthesia & Critical Care -*, 2008, **19**, 282–286, DOI: **10.1016/j.cacc.2008.09.015**.

7 Z. K. Zeleke, B. E. Moen and M. Bråtveit, Cement dust exposure and acute lung function: A cross shift study, *BMC Pulm. Med.*, 2010, **10**, 19, DOI: **10.1186/1471-2466-10-19**.

8 *Portland cement dust [MAK Value Documentation], the MAK-Collection for Occupational Health and Safety*, 2012, pp. 1–35, DOI: **10.1002/3527600418.mb6599715stae5315**.

9 R. Mirzaee, A. Kebriaei, R. Hashemi S, M. Sadeghi and M. Shahrakipour, Effects of exposure to Portland cement dust on lung function in Portland cement factory workers in Khash, Iran. Iran, *J. Environ. Health Sci. Eng.*, 2008, **5**, 201–206, DOI: **10.3889/oamjms.2018.233**.

10 A. K. M. Fell, H. Notø, M. Skogstad, K.-C. Nordby, W. Eduard, M. V. Svendsen, *et al.* A cross-shift study of lung function, exhaled nitric oxide and inflammatory markers in blood in Norwegian cement production workers, *Occup. Environ. Med.*, 2011, **68**, 799–805, DOI: **10.1136/oem.2010.057729**.

11 H. Kakooei, A. A. Kakouei, A. Poornajaf and F. Ferasaty, Variability in total dust exposure in a cement factory, *Ind. Health*, 2012, **50**, 64–68.

12 H. Kakooei, A. Gholami, M. Ghasemkhani, M. Hosseini, D. Panahi and G. Pouryaghoub, Dust Exposure and Respiratory Health Effects in Cement Production, *Acta Med. Iran.*, 2012, **50**, 122–126.

13 Z. K. Zeleke, B. E. Moen and M. Bråtveit, Lung function reduction and chronic respiratory symptoms among workers in the cement industry: a follow up study, *BMC Pulm. Med.*, 2011, **11**, 50, DOI: **10.1186/1471-2466-11-50**.

14 J. Mwaiselage, M. Bråtveit, B. Moen and M. Yost, Variability in Dust Exposure in a Cement Factory in Tanzania, *Ann. Occup. Hyg.*, 2005, **49**, 511–519, DOI: **10.1093/annhyg/mei013**.

15 L. C. Kenny, R. Aitken, C. Chalmers, J. F. Fabriès, E. Gonzalez-Fernandez, H. Kromhout, *et al.* A collaborative European study of personal inhalable aerosol sampler performance, *Ann. Occup. Hyg.*, 1997, **41**, 135–153, DOI: **10.1016/s0003-4878(96)00034-8**.

16 H. Notø, K.-C. Nordby and W. Eduard, Relationships between Personal Measurements of 'Total' Dust, Respirable, Thoracic, and Inhalable Aerosol Fractions in the Cement Production Industry, *Ann. Occup. Hyg.*, 2016, **60**, mev093, DOI: **10.1093/annhyg/mev093**.

17 H. Notø, K.-C. Nordby, H. Kjuus, Ø. Skare, Y. Thomassen and W. Eduard, Exposure to Thoracic Aerosol in a Prospective Lung Function Study of Cement Production Workers, *Ann. Occup. Hyg.*, 2014, **59**, 4–24, DOI: **10.1093/annhyg/meu080**.

18 ISO 7708, *Air Quality-Particle Size Fraction Definitions for Health Related Sampling*, International Standardization Organization, Geneva, Switzerland, 1995.

19 D. L. Bartley and J. H. Vincent, Sampling Conventions for Estimating Ultrafine and Fine Aerosol Particle Deposition in the Human Respiratory Tract, *Ann. Occup. Hyg.*, 2011, **55**, 696–709, DOI: **10.1093/annhyg/mer037**.

20 C. Hall and A. Hamilton, Porosities of building limestones: using the solid density to assess data quality, *Mater. Struct.*, 2016, **49**, 3969–3979, DOI: **10.1617/s11527-015-0767-3**.

21 R. M. Harrison, Airborne particulate matter, *Philos. Trans. R. Soc., A*, 2020, **378**, 20190319, DOI: **10.1098/rsta.2019.0319**.

22 M. Achternbosch, K. R. Bräutigam, N. Hartlieb, C. Kupsch, U. Richers and P. Stemmermann *et al.* Heavy metals in cement and concrete resulting from the co-incineration of wastes in cement kilns with regard to the legitimacy of waste utilisation. Karlsruhe, Germany: Forschungszentrum Karlsruhe GmbH Technik und Umwelt (Germany). Inst. fuer Technikfolgen-Abschaetzung und Systemanalyse (ITAS); *Forschungszentrum Karlsruhe GmbH Technik und Umwelt (Germany)*. Inst. fuer Technische Chemie, 2003.

23 J. Schindelin, I. Arganda-Carreras, E. Frise, V. Kaynig, M. Longair, T. Pietzsch, *et al.* Fiji: an open-source platform

1254 | *Environ. Sci.: Processes Impacts*, 2022, **24**, 1243–1256

This journal is © The Royal Society of Chemistry 2022

for biological-image analysis, *Nat. Methods*, 2012, **9**, 676–682, DOI: **10.1038/nmeth.2019**.

24 R-Core-Team, *A Language and Environment for Statistical Computing*, R Foundation for Statistical Computing, Vienna, Austria. 2020. **https://www.R-project.org/**.

25 M. Subbiah, *CoinMinD: Simultaneous Confidence Interval for Multinomial Proportion. 1.1*, edn,.2013.

26 C. P. Quesenberry and D. C. Hurst, Large Sample Simultaneous Confidence Intervals for Multinomial Proportions, *Technometrics*, 1964, **6**, 191–195, DOI: **10.2307/1266151**.

27 H. Wickham. *ggplot2: Elegant Graphics for Data Analysis*, Springer-Verlag, New York, 2016.

28 A. Kassambara, *ggpubr: 'ggplot2' Based Publication Ready Plots. R Package Version 0.4.0.999*, 2020.

29 N. Xiao. *ggsci: Scientific Journal and Sci-Fi Themed Color Palettes for 'ggplot2'. R Package Version 2.9*. 2018.

30 S. Eriksen Hammer, M. Ebert and S. Weinbruch, Comparison of operator- and computer-controlled scanning electron microscopy of particles from different atmospheric aerosol types, *Anal. Bioanal. Chem.*, 2019, **411**, 1633–1645, DOI: **10.1007/s00216-019-01614-7**.

31 P. Gwaze, H. J. Annegarn, J. Huth and G. Helas, Comparison of particle sizes determined with impactor, AFM and SEM, *Atmos. Res.*, 2007, **86**, 93–104, DOI: **10.1016/j.atmosres.2007.02.009**.

32 G. Rutkowska, M. Chalecki, P. Wichowski, J. Żwirska and B. Barszcz, Influence of siliceous and calcareous fly-ashes on properties of cement mortars, *J. Ecol. Eng.*, 2016, **17**, 280–288, DOI: **10.12911/22998993/64553**.

33 B. Berlinger, M. D. Bugge, B. Ulvestad, H. Kjuus, K. Kandler and D. G. Ellingsen, Particle size distribution of workplace aerosols in manganese alloy smelters applying a personal sampling strategy, *Environ. Sci.: Processes Impacts*, 2015, **17**, 2066–2073, DOI: **10.1039/C5EM00396B**.

34 T. K. Ervik, N. Benker, S. Weinbruch, Y. Thomassen, D. G. Ellingsen and B. Berlinger, Size distribution and single particle characterization of airborne particulate matter collected in a silicon carbide plant, *Environ. Sci.: Processes Impacts*, 2019, **21**, 564–574, DOI: **10.1039/C8EM00518D**.

35 H.-S. Kwon, M. H. Ryu and C. Carlsten, Ultrafine particles: unique physicochemical properties relevant to health and disease, *Exp. Mol. Med.*, 2020, **52**, 318–328, DOI: **10.1038/s12276-020-0405-1**.

36 T. Ferge, J. Maguhn, H. Felber and R. Zimmermann, Particle Collection Efficiency and Particle Re-entrainment of an Electrostatic Precipitator in a Sewage Sludge Incineration Plant, *Environ. Sci. Technol.*, 2004, **38**, 1545–1553, DOI: **10.1021/es034709s**.

37 A. Noël, G. L'Esperance, Y. Cloutier, P. Plamondon, J. Boucher, S. Philippe, *et al.* Assessment of the Contribution of Electron Microscopy to Nanoparticle Characterization Sampled with Two Cascade Impactors, *J. Occup. Environ. Hyg.*, 2013, **10**, 155–172, DOI: **10.1080/15459624.2012.760391**.

38 M. Gensch and A. P. Weber, Rebound behavior of nanoparticle-agglomerates, *Adv. Powder Technol.*, 2017, **28**, 1930–1942, DOI: **10.1016/j.apt.2017.05.003**.

39 Y.-S. Cheng and H.-C. Yeh, Particle bounce in cascade impactors, *Environ. Sci. Technol.*, 1979, **13**, 1392–1396, DOI: **10.1021/es60159a017**.

40 L. G. Cena, W. P. Chisholm, M. J. Keane, A. Cumpston and B. T. Chen, Size Distribution and Estimated Respiratory Deposition of Total Chromium, Hexavalent Chromium, Manganese, and Nickel in Gas Metal Arc Welding Fume Aerosols, *Aerosol Sci. Technol.*, 2014, **48**, 1254–1263, DOI: **10.1080/02786826.2014.980883**.

41 M. A. Reuter, K. Heiskanen, U. Boin, A. Van Schaik, E. Verhoef and Y. Yang *et al.*, *Aluminium Metal Production. Developments in Mineral Processing*, The Netherlands Elsevier, Amsterdam, 2005, pp. 391–451.

42 R. Feige and G. Merker. *Use of Recovered Alumina from Aluminium Slags in Refractories for Aluminium. Internationalen Feuerfest-Kolloquium*, Germany Verlag Stahleisen GmbH, Düsseldorf, 1998.

43 E. Worrell and M. Reuter, *Handbook of Recycling: State-Of-The-Art for Practitioners, Analysts, and Scientists*, Elsevier, Waltham, MA, USA, 2014.

44 MdM. Cortada Mut, L. K. Nørskov, F. J. Frandsen, P. Glarborg and K. Dam-Johansen, Review: Circulation of Inorganic Elements in Combustion of Alternative Fuels in Cement Plants, *Energy Fuels*, 2015, **29**, 4076–4099, DOI: **10.1021/ef502633u**.

45 C. Twomey, C. Birkinshaw and S. Breen, The identity of the sulfur-containing phases present in cement clinker manufactured using a high sulfur petroleum coke fuel, *J. Chem. Technol. Biotechnol.*, 2004, **79**, 486–490, DOI: **10.1002/jctb.1008**.

46 P. J. Jackson. 2 - Portland Cement: Classification and Manufacture, in, *Lea's Chemistry of Cement and Concrete*, ed. P.C. Hewlett, 4th edn, Butterworth-Heinemann, Oxford, 1998, pp. 25–94.

47 M. Maslehuddin, O. S. B. Al-Amoudi, M. K. Rahman, M. R. Ali and M. S. Barry, Properties of cement kiln dust concrete, *Constr. Build. Mater.*, 2009, **23**, 2357–2361, DOI: **10.1016/j.conbuildmat.2008.11.002**.

48 H. S. Abdelgader, M. Amran, M. Kurpińska, M. A. Mosaberpanah, G. Murali and R. Fediuk. 10 - Cement kiln dust, in *Sustainable Concrete Made with Ashes and Dust from Different Sources*, ed. R. Siddique, R. Belarbi, Woodhead Publishing, 2022. pp. 451–79.

49 P. Hawkins, P. Tennis, and R. Detwiler, *The Use of Limestone in Portland Cement: A State-Of-The-Art Review*, Portland Cement Association, Illinois, USA, 2003.

50 K. L. Scrivener, *The Development of Microstructure during the Hydration of Portland Cement [PhD Thesis]*, Imperial College London, London, GB, 1984.

51 P. Stutzman, *Direct Determination of Phases in Portland Cements by Quantitative X-Ray Powder Diffraction*, National Institute of Standards and Technology, Gaithersburg, US, 2010.

52 A. Marzouki, A. Lecomte, A. Beddey, C. Diliberto and M. Ben Ouezdou, The Effects of grinding on the properties of Portland-limestone cement, *Constr. Build. Mater.*, 2013, **48**, 1145, DOI: **10.1016/j.conbuildmat.2013.07.053**.

53 C. Misra, M. Singh, S. Shen, C. Sioutas and P. M. Hall, Development and evaluation of a personal cascade impactor sampler (PCIS), *J. Aerosol Sci.*, 2002, **33**, 1027–1047, DOI: **10.1016/S0021-8502(02)00055-1**.

54 S. Bau and O. Witschger, A modular tool for analyzing cascade impactors data to improve exposure assessment to airborne nanomaterials, *J. Phys.: Conf. Ser.*, 2013, **429**, 012002, DOI: **10.1088/1742-6596/429/1/012002**.

55 H. Notø, Y. Thomassen, W. Eduard, H. Kjuus, K.-C. Nordby and Ø. Skare, Exposure to Thoracic Aerosol in a Prospective Lung Function Study of Cement Production Workers, *Ann. Occup. Hyg.*, 2014, **59**, 4–24, DOI: **10.1093/annhyg/meu080**.

56 K.-C. Nordby, H. Notø, W. Eduard, M. Skogstad, A. K. Fell, Y. Thomassen, *et al.* Thoracic dust exposure is associated with lung function decline in cement production workers, *Eur. Respir. J.*, 2016, **48**, 331–339, DOI: **10.1183/13993003.02061-2015**.

57 B. Asgharian, A Model of Deposition of Hygroscopic Particles in the Human Lung, *Aerosol Sci. Technol.*, 2004, **38**, 938–947, DOI: **10.1080/027868290511236**.

58 D. Bwalya, M. Bråtveit and B. E. Moen, Chronic Respiratory Symptoms Among Workers at a Limestone Factory in Zambia, *Arch. Environ. Occup. Health*, 2011, **66**, 47–50, DOI: **10.1080/19338244.2010.506498**.

59 National Center for Biotechnology Information, *PubChem Compound Summary for CID 10112, Calcium carbonate*, **https://pubchem.ncbi.nlm.nih.gov/compound/Calcium-carbonate**, accessed Nov. 21, 2021.

60 A. K. M. Fell and K. C. Nordby, Association between exposure in the cement production industry and non-malignant respiratory effects: a systematic review, *BMJ Open*, 2017, **7**, e012381, DOI: **10.1136/bmjopen-2016-012381**.

1256 | *Environ. Sci.: Processes Impacts*, 2022, **24**, 1243–1256

This journal is © The Royal Society of Chemistry 2022